Desantes J.M.; López, JJ.; Novella Rosa, R.; Beltrao De Vargas-Antolini, J. (2021). Pre-chamber ignition systems: A methodological proposal to reproduce a reference case in a simplified experimental facility for fundamental studies. International Journal of Engine Research. 22(11):3358-3371. https://doi.org/10.1177/1468087420971115

Pre-chamber ignition systems: a methodological proposal to reproduce a reference case in a simplified experimental facility for fundamental studies

José M. Desantes[a], **J. Javier López**[a*], **Ricardo Novella**[a], and **Jácson Antolini**[a]

[a]CMT - Motores Térmicos, Universitat Politècnica de València, Camino de Vera s/n, 46022 Valencia, Spain

Corresponding author (*):

Abstract

To further understand the processes and phenomena taking place in the pre-chamber (PC) ignition concept, many studies under simplified conditions have been carried out in different experimental facilities (e.g. constant volume chambers and rapid compression machines). However limited information is provided about how the volume, orifice diameter and number of orifices were defined, raising the question whether the results are representative of engine-like conditions or not. This novel study arises from the necessity to determine a methodology to reproduce a reference pre-chamber, preserving as much as possible its jet characteristics. A theoretical development based on the first law of thermodynamics has been performed, and a relationship between the effective flow area, pre-chamber volume and engine speed is proposed as the governing parameter of the mass exchange between chambers. Besides, relaying on the know-how of gas jets, a relationship between the orifice diameter, jet tip penetration and engine speed is suggested as the criterion to preserve the relative jet penetration (respect to the distance from the PC hole to the combustion chamber walls). A numerical validation of these assumptions was carried out using a one-dimensional flow calculator to estimate the thermodynamic properties and mass transfer between chambers, and a one-dimensional spray model to estimate the penetration of the PC combustion products jets. Finally, preserving the ratio between the total area of the PC holes and the product of the PC volume and the engine speed for two pre-chamber geometries, an identical pressure rise rate, in an angular basis, is achieved in both pre-chambers. Furthermore, the same relative jet penetration rate, in an angular basis, can be also achieved, even under different engine speeds, when the ratio between the orifice diameter and the product of the square of the jet free length and the engine speed is preserved.

Keywords

Turbulent jet ignition; Torch ignition; Pre-chamber design; Spark-ignition engine.

1. Introduction

The pre-chamber ignition concept, also known as Turbulent Jet Ignition (TJI), consists of a small volume chamber, where the spark plug is located, connected to a bigger volume (main) chamber through orifices. When this small volume (1 to 5% of the clearance volume) is ignited, the combustion products are ejected to the main chamber, promoting a fast burn of the main charge [1]. This increment of the burn rate due to the increase of ignition spots, enables to shorten the combustion duration up to 3 times [2], and also to increase the compression ratio [3,4].

Pre-chambers (PC) can have additional air and/or fuel supply or not. On the one hand, if the pre-chamber scavenge process depends on the main chamber scavenge process, i.e. there is not a dedicated air intake to promote the pre-chamber scavenge, it is called unscavenged PC. On the contrary, if there is a dedicated air intake to scavenge the pre-chamber, it is referred as scavenged PC. On the other hand, if there is an additional fuel supply directly into the pre-chamber, enabling a richer mixture in this one, it is called an active system (otherwise, it is referred as passive system). The active approach allows achieving ultra-lean conditions at the main chamber without the ignitability problems of lean mixtures in the pre-chamber [5].

With these features, this concept becomes an efficient method to initiate the combustion process of the main charge at unfavorable conditions, as diluted mixtures (either with air or EGR) and/or large bore engines [6,7]. Such conditions require a more powerful and spatially well-distributed ignition source than the conventional spark plug to ensure a proper flame development and combustion stability [4].

Collecting pre-chamber data under real engine conditions may be a challenge due to the lack of physical space, making it difficult to place a pressure sensor or an optical access. For this reason, to allow the access to such information, some studies are performed on experimental facilities[1,5,8–15], rather than in real engines, with the drawback of reproducing the phenomenon under simplified conditions. The main differences between the conditions in a real engine and an experimental facility can occur in several aspects and levels, such as: on the thermodynamic conditions, mixture composition (e.g. residual gas fraction), flow pattern (e.g. turbulence level and orientation), geometrical aspects (e.g. pre- to main chamber volume ratio, surface area to volume ratio and orifice diameter), etc. Regarding the geometrical aspects, limited information is available in the literature about how the volume, orifice diameter and number of orifices were defined in these simplified conditions, raising the question whether the results are representative of engine-like conditions or not.

To start analyzing the concept and to define the better approach to emulate it, it is mandatory to identify the main processes taking place in an unscavenged pre-chamber, which are: scavenge and filling with fresh mixture, combustion, possible flame quenching at the orifices, jet ejection and main chamber ignition. In real engine operation these processes are cyclic and interdependent, as well as highly affected by the PC volume, orifice diameter, number of orifices and engine speed. Thus, it is necessary to establish a criterion to define these parameters when a baseline pre-chamber wants to be tested under simplified conditions (e.g. single orifice, and/or different pre-chamber volume, and/or different engine speed, and/or different main chamber characteristic length, etc.).

From a fundamental point of view, the mass transfer phenomena between the pre- and main chamber, either during the filling or the jet ejection period, is governed by the pressure drop, the effective flow area, and the local thermodynamic conditions. Taking the filling period as an example, the main chamber thermodynamic conditions are determined, as a first approach, by the compression ratio, whereas those in the pre-chamber depend on the incoming mass flow rate. The latter, however, is affected by the rate of volume change, associated to the engine speed, and may be limited if chocked conditions are reached at the orifices. In the meantime, the flow area of the pre-chamber offers a resistance to the flow passage, causing a pressure difference between the volumes connected by them. Therefore, there is a compromise between geometrical pre-chamber aspects and engine operating parameters. During the combustion process, however, the pressure rise will also change according to the energy delivered by the fuel, defined by the chemical energy released (Q_{ch}), and the heat losses.

Geometrical pre-chamber aspects have been studied by some authors. Ashish Shah et al. [16,17] for instance, investigated the effect of the nozzle area ratio (defined as the ratio of the nozzles

total area to the pre-chamber volume, in cm^{-1}) in two different engines: a heavy duty engine operating at 1200 rpm and a large bore marine engine operating at 800 rpm. The authors found discrepancies between the engines regarding main chamber combustion duration and flame development angle, even preserving the nozzle area ratio. Corrections to compensate the differences in terms of induced flow patterns (e.g. swirl and squish), caused by differences in engine speed and combustion chamber geometry were applied too. The results, therefore, reveal that the similarity of pre-chambers cannot be achieved only preserving this nozzle area ratio.

In another study, performed by R.B.R. da Costa et al. [18], a thermodynamic diagnostic model was developed to determine the energy released to the main chamber, essentially during the closed cycle. The combustion in the two chambers was modeled independently according to a Wiebe function. The mass flow rate between the chambers was assumed as an isentropic and compressible flow. The authors described how the energy flow between the chambers is, as well as the angular evolution of the temperature and pressure in both chambers. Additionally, they presented a parameter to relate the pre-chamber geometrical parameters (volume and nozzle area) to the engine operating speed, the latter without any explicit reasoning.

S. Biswas et al. [19] studied the effect of the pre-chamber orifice diameter on the ignition mechanisms, namely flame ignition and jet ignition. Flame ignition is considered when the hot jet coming out from the pre-chamber contains flame kernels and intermediate species that promote chain-branching (OH radical, for instance), whereas jet ignition is considered when the jet is made of hot combustion products only, with very little or no OH radicals. The main result of this study was that decreasing the orifice diameter switches the ignition mechanism from flame ignition to jet ignition, provided that the volume and initial thermodynamic conditions are kept constant. This result suggests that the higher turbulence intensity (higher jet velocity) and the lower integral scale (smaller orifice diameter), both leading to a lower Damköhler number, pushes the operating point towards the broken reaction zone.

Many other authors investigated the pre-chamber performance by changing the pre-chamber volume or orifice number and dimensions (diameter and length), observing either the global engine performance [20–23], or the jet characteristics (in this last case either in test rigs at low pressure and temperature [9,24], or at engine-like thermodynamic conditions [10,13,25]).

G. Gentz et al. [12], M. Gholamisheeri et al. [10,26] and S. Biswas et al. [19] studied the jet characteristics and main chamber ignition of single orifice pre-chambers from a more fundamental point of view. Although it goes in the opposite direction compared to the pre-chambers used in production engines, single orifice pre-chambers studies are necessary to understand intrinsic jet phenomena, isolating the effect of jet interaction. Nevertheless, to transfer this information to engine applications, it is desired that these jets together with the boundary conditions are like those found in engines. Hence, besides the thermodynamic conditions (high pressure and high temperature), the jet flow pattern has to be scaled in terms of velocity and characteristic length. Regarding the combustion process, the Damköhler number is a useful ratio to quantify the importance of the reaction rate in relation to the diffusion rate. Therefore, for the same fuel composition, to maintain the Damköhler number of the jets (of the single orifice pre-chamber and of the real engine pre-chamber, which are intended to be similar in terms of behavior), the local values of the integral scale and the turbulence intensity must be scaled to maintain the diffusion rate between these jets. This idea is, probably, the one that has promoted most of the current research, the objective of which is to establish a relationship between the pre-chamber geometry and the engine operating parameters, which later can be used to determine how some given pre-chamber and operating point can be emulated in a single orifice pre-chamber for fundamental research purposes.

Therefore, the present work aims to define a methodology to determine the geometrical parameters of a pre-chamber to be designed for an experimental facility (e.g. Rapid Compression-Expansion Machine), focusing on emulating a multi-orifice reference pre-chamber into a single orifice configuration, due to the better visualization and to avoid jet interaction.

The structure of the paper is the following: first, the methodology and validation tools are presented. Then, the PC filling and emptying processes are analyzed, where a relationship between geometrical pre-chamber aspects and engine operating parameters is theoretically presented. Next, this relationship is validated in terms of the thermodynamic conditions at both

pre and main chambers. After that, the jet penetration and orifice quenching issues are briefly discussed. Finally, the conclusions of this study are shown.

2. Research approach and validation tools

2.1. Research approach

The present study was divided in two parts: a theoretical development and a computational validation. The theoretical development presents some relations that governs the pre-chamber filling and jet ejection processes, as well as the jet tip penetration and the flame quenching in the orifices, whereas two computational tools were used to validate the thermodynamic and mass flow aspects (GT-Power) and the jet characteristics (DICOM), both explained in section 2.2.

Looking at the pre-chamber ignition concept processes separately, it is possible to identify the crucial elements of each one, which are:

- Pre-chamber filing: During this phase, the fresh charge coming from the main chamber is transferred to the pre-chamber in a rate defined by the flow velocity (note that this one may be limited if sonic conditions at the orifice are reached) and the total orifice area. This mass flow causes an increase in PC pressure.
- Pre-chamber scavenging: Concomitant with the PC filling process, the scavenge process itself depends on the flow pattern generated by the orifices. Therefore, it is a process completely related to three-dimensional phenomena.
- Pre-chamber combustion: Started by a sparkplug, it shares the same difficulties than a conventional SI engine, being highly affected by residual gases, equivalence ratio and local turbulent kinetic energy. Besides, the higher surface to volume ratio in comparison to the main chamber implies non-negligible heat losses to the walls.
- Pre-chamber ejection: Overlapped with the PC combustion, this process consists of the ejection of gases into the main chamber. Initially the unburnt mixture acts as a turbulence source, then the hot gases act as both an ignition and a turbulence source [27]. The PC flame front can be quenched or not at the orifice, depending mainly on its diameter and equivalence ratio [8,19].
- Jet penetration: It is reasonable to think that different engine sizes (i.e. cylinder bore) require different penetration rates (mainly governed by the momentum at the orifice exit) to ensure a proper combustion duration. Thus, the expectation is that the orifice diameter should be scaled with the distance between the PC and the cylinder walls.

Even though charge stratification (e.g. composition and temperature) and three-dimensional phenomena (e.g. turbulence) do play an important role in the pre-chamber combustion process, these factors are not going to be accounted for in the reasoning shown in this study. Moreover, thanks to the possibility to completely scavenge the combustion chamber before a combustion cycle on experimental facilities (e.g. Rapid Compression-Expansion Machine), the PC scavenge process will also not be accounted for. Therefore, this work is going to discuss exclusively 0D (and 1D for some aspects) phenomena, such as PC filling (section 3.1.1), PC ejection (section 3.1.2), jet penetration (section 4), and flame quenching (section 5).

2.2. Validation tools

2.2.1. Thermodynamic and mass flow validation

A GT-Power model was used to solve the continuity, momentum and energy equations during the closed cycle (from inlet valve closing -IVC-, until exhaust valve opening -EVO-). The heat transfer was modeled according to Woschni's correlation. Additionally, since the prediction of the main chamber ignitability is not necessary now, the main chamber combustion object was neglected, and the downstream jet condition during ejection is simply a non-ignited hot chamber. On the contrary, the pre-chamber combustion process needs to be correctly described, because of its vital influence on the pre-chamber behavior. In this study, it was represented by a Wiebe function (later it will be shown that this arbitrary choice does not affect the validity of the conclusions), ensuring the same combustion profile for all cases, except when it was intentionally changed to highlight its effect on the pressure rise rate. Both the duration and the shape of this combustion law were determined based on some available experimental data [28].

The initial conditions were imposed both in the main chamber and the pre-chamber at IVC, and one single cycle was calculated using the explicit solver. The composition chosen was a stoichiometric mixture between air and methane, and no residual or EGR gases were added. More details about the engine geometry and initial conditions are described in Table 1.

Table 1. Engine specifications and initial conditions.

Engine	4-stroke SI
Stroke x Bore [mm]	80 x 80.5
Compression Ratio [-]	13.4:1
IVC [CAD]	-120 ATDC
EVO [CAD]	160 ATDC
Clearance Volume [cm^3]	32.632
Temperature at IVC [K]	320.0
Pressure at IVC [bar]	1.0
Composition at IVC [mass fraction]	CH_4 = 0.055
	O_2 = 0.220
	N_2 = 0.725

The discharge coefficient of the pre-chamber orifices was set to 1 for all cases, avoiding the effect of nozzle diameter variation in the discharge coefficient.

2.2.2.Jet characteristics validation

In addition to orifice mass flow rate, jet velocity and momentum, a more complete assessment of the jet characteristics can be done by estimating a “hypothetical” jet penetration rate, which gives some idea about how far and fast the jet leading edge could go at a given time. The term “hypothetical” has been used intentionally because, in a real situation, the jet ignites the main chamber charge while it is penetrating and entraining fresh mixture, which greatly increases the complexity of the problem, requiring Computational Fluid Dynamics (CFD) calculations and detailed chemical kinetics to more accurately predict it [29].

To estimate this hypothetical jet penetration rate, a one-dimensional spray model was used. This code, developed at CMT-Motores Térmicos, predicts the evolution of a steady or transient turbulent jet or spray, either inert or reactive. The model development, solution procedure and more details about the model can be found in [30,31].

In the current study, the transient input data to this spray model were imported from GT-Power and the same boundary conditions were imposed. The jet morphology (mainly cone angle) was considered the same for all pre-chamber geometries, since it is intended to test similar orifice geometries. Swirl and/or any other type of engine-induced air movement was not considered.

3. PC filling and ejection processes

3.1. Theoretical development

This section demonstrates some geometrical relations and combustion parameters that are important in the frame of pre-chamber design, especially for reciprocating internal combustion engine applications. At the same time, it develops a methodology to reproduce the same characteristics, in terms of pre-chamber filling and jet ejection, of a multi-orifice pre-chamber in a single-orifice pre-chamber, even if the engine speed is different.

Starting from the energy conservation equation, the objective is to point out the main variables that affect the energy flow during the pre-chamber filling and combustion processes, and how they are related to the pressure and temperature rise rate.

To perform this evaluation, two control volumes (open systems) were defined: the main chamber control volume (CV_{MC}) and the pre-chamber control volume (CV_{PC}). The CV_{MC} is surrounded by a moving control surface, which follows the piston movement, whereas the CV_{PC} is surrounded by a fixed control surface, due to its constant volume. No mass transfer beyond the pre-chamber and the main chamber is assumed. Figure 1 shows schematically the control volumes and their main properties.

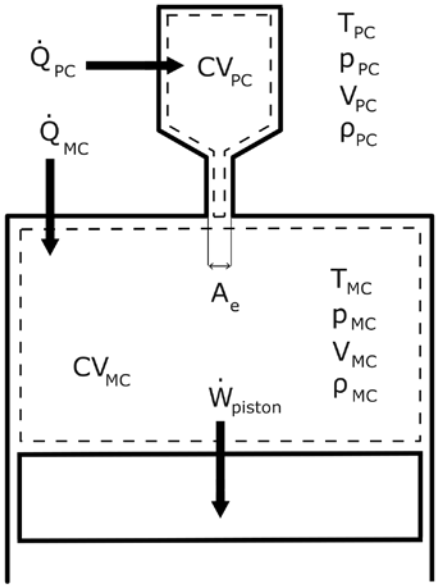

Figure 1 – Control volume scheme.

Considering that the energy in both control volumes is essentially thermal energy (both kinetic and potential energy are neglected *in the control volumes*) and that the potential energy associated to the mass flow is negligible too (but here the kinetic energy is considered), the energy variation in the control volume (open system) can be defined as:

$$\frac{dE_{CV}}{dt} = \frac{dU_{CV}}{dt} = \frac{dQ_{CV}}{dt} - \frac{dW_{CV}}{dt} + \frac{dm_{CV}}{dt}\left(h_k + \frac{v^2}{2}\right) \qquad 3.1$$

where E_{CV} is the total energy in the control volume, U_{CV} is the internal energy in the control volume, Q_{CV} is the net heat added to the control volume, W_{CV} is the work done by the control volume, $\frac{dm_{CV}}{dt}$ is the mass flow rate across the control surface, h_k is the enthalpy corresponding to the mass being transferred, and v is the flow velocity at the orifice.

Moreover, the internal energy can be calculated as:

$$U = mc_v T \qquad 3.2$$

where c_v is the specific heat at constant volume. If the time derivative is performed, the internal energy variation in a control volume is given by:

$$\frac{dU_{CV}}{dt} = c_{v,CV} T_{CV} \frac{dm_{CV}}{dt} + m_{CV} c_{v,CV} \frac{dT_{CV}}{dt} \tag{3.3}$$

The second term at the right-hand side can be rewritten using the equation of state (Equation 3.4) and its time derivative (Equation 3.5), as follows:

$$P_{CV} V_{CV} = m_{CV} R T_{CV} \quad \Rightarrow \quad T_{CV} = \frac{P_{CV} V_{CV}}{m_{CV} R} \tag{3.4}$$

$$\frac{dT_{CV}}{dt} = \frac{V_{CV}}{m_{CV} R} \frac{dP_{CV}}{dt} - \frac{P_{CV} V_{CV}}{R m_{CV}{}^2} \frac{dm_{CV}}{dt} + \frac{P_{CV}}{m_{CV} R} \frac{dV_{CV}}{dt} \tag{3.5}$$

$$\frac{dU_{CV}}{dt} = C_{v,CV} T_{CV} \frac{dm_{CV}}{dt} + C_{v,CV} \left(\frac{V_{CV}}{R} \frac{dP_{CV}}{dt} - \frac{P_{CV} V_{CV}}{R m_{CV}} \frac{dm_{CV}}{dt} + \frac{P_{CV}}{R} \frac{dV_{CV}}{dt} \right) \tag{3.6}$$

Thus, rearranging some terms, the internal energy variation in a control volume becomes:

$$\frac{dU_{CV}}{dt} = \frac{c_{v,CV}}{R} \left(V_{CV} \frac{dP_{CV}}{dt} + P_{CV} \frac{dV_{CV}}{dt} \right) \tag{3.7}$$

Now, Equation 3.1 can be rewritten as:

$$\frac{dE_{CV}}{dt} = \frac{c_{v,CV}}{R} \left(V_{CV} \frac{dP_{CV}}{dt} + P_{CV} \frac{dV_{CV}}{dt} \right) = \frac{dQ_{CV}}{dt} - \frac{dW_{CV}}{dt} + \frac{dm_{CV}}{dt} \left(h_k + \frac{v^2}{2} \right) \tag{3.8}$$

which represents the energy balance in a control volume. Now this equation will be applied to both control volumes, CV_{PC} and CV_{MC}, to obtain Eqs. 3.9 and 3.10, under the following hypotheses:

I. No work is performed by CV_{PC}.
II. No volume variation takes place in CV_{PC}.

$$\frac{dE_{PC}}{dt} = \frac{c_{v,PC}}{R} V_{PC} \frac{dP_{PC}}{dt} = \frac{dQ_{ch,PC}}{dt} - \frac{dQ_{ht,PC}}{dt} + \frac{dm_{CV}}{dt} \left(h_k + \frac{v^2}{2} \right) \tag{3.9}$$

$$\begin{aligned} \frac{dE_{MC}}{dt} &= \frac{c_{v,MC}}{R} \left(V_{MC} \frac{dP_{MC}}{dt} + P_{MC} \frac{dV_{MC}}{dt} \right) \\ &= \frac{dQ_{ch,MC}}{dt} - \frac{dQ_{ht,MC}}{dt} - \frac{dW_{piston}}{dt} + \frac{dm_{CV}}{dt} \left(h_k + \frac{v^2}{2} \right) \end{aligned} \tag{3.10}$$

where, $Q_{ch,i}$ is the chemical energy released by the fuel combustion in the control volume i, $Q_{ht,i}$ are the heat losses to the walls in the control volume i and W_{Piston} is the work done by the piston on the control volume. The enthalpy sub index k depends on the mass flow orientation: if it is a positive value (i.e. mass entering into the control volume) the reference are the conditions at the opposite control volume (for instance, when the mass is flowing to the pre-chamber, the enthalpy reference are the main chamber conditions).

In the following subsections, particularizations of Equations 3.9 and 3.10 are going to be presented for the pre-chamber filling process and the pre-chamber combustion (jet ejection) process.

3.1.1. Pre-chamber filling process

The pre-chamber filling process is defined as the period between the IVC and the angle were the PC pressure overcomes that in the MC. As a first approach, this last angle can be taken when the start of combustion (SOC) in the PC takes place. Therefore, it comprises the period in which the pre-chamber is filled with fresh mixture coming from the main chamber, and no combustion

at all occurs nor in the PC, nor in the MC. For this reason, the following additional hypotheses for the pre-chamber filling process can be taken:

I. No combustion occurs both in CV_{PC} and CV_{MC}.
II. The mass is flowing from CV_{MC} to CV_{PC}, thus the enthalpy sub index would be $k = MC$.

With these hypotheses, equations 3.9 and 3.10 become:

$$\frac{c_{v,PC}}{R} V_{PC} \frac{dP_{PC}}{dt} = -\frac{dQ_{ht,\,PC}}{dt} + \frac{dm_{MC}}{dt}\left(h_{MC} + \frac{v^2}{2}\right) \tag{3.11}$$

$$\frac{c_{v,MC}}{R}\left(V_{MC}\frac{dP_{MC}}{dt} + P_{MC}\frac{dV_{MC}}{dt}\right) = -\frac{dQ_{ht,\,MC}}{dt} - \frac{dW_{piston}}{dt} - \frac{dm_{MC}}{dt}\left(h_{MC} + \frac{v^2}{2}\right) \tag{3.12}$$

These equations can be numerically solved using either implicit or explicit methods. However, as the objective of the present study is to point out the main variables affecting the PC filing process, an approximation of the mass flow rate between chambers can be made assuming an isentropic flow through an orifice, calculated as:

$$\frac{dm}{dt} = A_e\left[2\rho_{up}\left(P_{up} - P_{down}\right)\right]^{\frac{1}{2}} \varphi \; ; \; A_e = C_D A_n \tag{3.13}$$

where A_e is the effective area, A_n is the nozzle area (i.e. the sum of orifice cross section areas), C_D is the discharge coefficient, ρ is the density, and φ is the compressibility factor, defined as follows:

$$\varphi = \left\{ \frac{\left(\frac{\gamma}{\gamma-1}\right)\left[\left(\frac{P_{down}}{P_{up}}\right)^{\frac{2}{\gamma}} - \left(\frac{P_{down}}{P_{up}}\right)^{\frac{\gamma+1}{\gamma}}\right]}{1 - \frac{P_{down}}{P_{up}}} \right\}^{\frac{1}{2}} \tag{3.14}$$

where γ is the ratio of specific heats, and the subscript up and $down$ refers to the conditions upstream and downstream the orifice, respectively. Thus, the mass flow rate from CV_{MC} to CV_{PC}, according to Equation 3.13, can be estimated as:

$$\frac{dm_{MC}}{dt} = A_e\left[2\rho_{MC}\left(P_{MC} - P_{PC}\right)\right]^{\frac{1}{2}} \varphi \; ; \; A_e = C_D A_n \tag{3.15}$$

Appling Equation 3.15 into Equation 3.11 and rearranging terms, the pre-chamber pressure rise rate can be expressed in terms of the effective flow area and the PC volume:

$$\frac{dP_{PC}}{dt} = \frac{\boldsymbol{A_e}}{\boldsymbol{V_{PC}}} \frac{R}{c_{v,PC}} \left[2\rho_{MC}\left(P_{MC} - P_{PC}\right)\right]^{\frac{1}{2}} \varphi \left(h_{MC} + \frac{v^2}{2}\right) - \frac{R}{V_{PC}\, c_{v,PC}} \frac{dQ_{ht,\,PC}}{dt} \tag{3.16}$$

The equations presented until now are all described in terms of time. However, in reciprocating internal combustion engine applications, it might be more useful to describe them in crank angle basis, which introduces an important characteristic time: the engine speed (N, in rpm; n, in rps). Thus, the time variation can be written in terms of crank angle degrees (θ) as follows:

$$t = \theta \frac{1}{n(rps)} \frac{1}{360} = \theta \frac{1}{N(rpm)} \frac{1}{6} \tag{3.17}$$

If Equation 3.17 is differentiated, the relationship between dt and $d\theta$ can be found:

$$dt = d\theta \frac{1}{N(rpm)} \frac{1}{6} \tag{3.18}$$

Rewriting Equation 3.16 in crank angle basis:

$$\frac{dP_{PC}}{d\theta} = \frac{1}{6\,\boldsymbol{N}} \left\{ \frac{\boldsymbol{A_e}}{\boldsymbol{V_{PC}}} \frac{R}{c_{v,PC}} [2\rho_{MC}(P_{MC} - P_{PC})]^{\frac{1}{2}}\, \varphi \left(h_{MC} + \frac{v^2}{2} \right) - \frac{R}{V_{PC}\, c_{v,PC}} \frac{dQ_{ht,\,PC}}{d\theta} \right\} \tag{3.19}$$

Therefore, the pre-chamber pressure rise rate is a function of the thermodynamic conditions of both chambers, as well as the heat losses to the walls, the effective flow area, the pre-chamber volume and the engine speed. Assuming that a given pre-chamber pressure rise rate is intended to be reproduced in a new engine or a new PC configuration, and that the heat losses term is small compared to the other terms in the equation (this will be demonstrated later, during the validation section), the following actions might be taken. First, to preserve the angular evolution of the main chamber thermodynamic conditions (ρ, h and P, all of them appearing in the equation), the engine compression ratio must be kept the same. Then, to preserve the thermodynamic conditions at the pre-chamber (P and $dP/d\theta$), it is necessary to keep the parameter $A_e/(V_{PC}\, N)$. With this last criterion the mass flow rate is scaled according to the pre-chamber volume and engine speed, by introducing a variation in the effective flow area. Thereby, the energy flux in terms of enthalpy and kinetic energy associated to the mass flow is scaled, and a similar pressure rise rate is achieved in both pre-chambers with this new configuration.

3.1.2.Pre-chamber ejection process

As a complement to the previous sub-section, where the pre-chamber filling process was studied, the following analysis will evaluate the period from the pre-chamber SOC until the EVO. This phase comprises the period in which the pre-chamber mixture is ignited and the hot combustion products are ejected to the main chamber.

Now, the following additional hypotheses for the pre-chamber combustion process can be assumed:

I. No combustion occurs in CV_{MC}.
II. The mass is flowing from CV_{PC} to CV_{MC}, thus the enthalpy sub index would be $k = PC$.

If the previous hypotheses are considered in Eqs. 3.9 and 3.10, they become, respectively:

$$\frac{c_{v,PC}}{R} V_{PC} \frac{dP_{PC}}{dt} = \frac{dQ_{ch,\,PC}}{dt} - \frac{dQ_{ht,\,PC}}{dt} - \frac{dm_{PC}}{dt} \left(h_{PC} + \frac{v^2}{2} \right) \tag{3.20}$$

$$\begin{aligned} &\frac{c_{v,MC}}{R} \left(V_{MC} \frac{dP_{MC}}{dt} + P_{MC} \frac{dV_{MC}}{dt} \right) \\ &= \frac{dQ_{ch,\,MC}}{dt} - \frac{dQ_{ht,\,MC}}{dt} - \frac{dW_{piston}}{dt} + \frac{dm_{PC}}{dt} \left(h_{PC} + \frac{v^2}{2} \right) \end{aligned} \tag{3.21}$$

Using the approximation to the mass flow rate as an isentropic flow through an orifice (Equation 3.13), the energy variation in CV_{PC} becomes:

$$\frac{c_{v,PC}}{R} V_{PC} \frac{dP_{PC}}{dt} = \frac{dQ_{ch,\,PC}}{dt} - \frac{dQ_{ht,\,PC}}{dt} - A_e [2\rho_{PC}(P_{PC} - P_{MC})]^{\frac{1}{2}}\, \varphi \left(h_{PC} + \frac{v^2}{2} \right) \tag{3.22}$$

Rewriting in a crank angle basis and rearranging terms, the pre-chamber pressure rise rate during pre-chamber combustion can be expressed as:

$$\frac{dP_{PC}}{d\theta} = \frac{R}{C_v}\rho_{PC}\,(F/A)_{stoich}\,F_R LHV\,\frac{dx_{b,PC}}{d\theta} - \frac{\boldsymbol{A_e}}{\boldsymbol{V_{PC}N}}\frac{R}{C_v}\frac{1}{6}[2\rho_{PC}(P_{PC}-P_{MC})]^{\frac{1}{2}}\,\varphi\left(h_{PC}+\frac{v^2}{2}\right) - \frac{R}{V_{PC}\,c_{v,PC}}\frac{dQ_{ht,\,PC}}{dt} \quad 3.23$$

where R is the gas constant, F_R is the fuel-to-air equivalence ratio, LHV is the Lower Heating Value of the fuel, and $x_{b,PC}$ is the fuel mass fraction burned at CV_{PC}, which can be approximated by a Wiebe function [32]:

$$x_b = 1 - exp\left[-a\left(\frac{\theta-\theta_0}{\Delta\theta}\right)^{m_{Wiebe}+1}\right] \quad 3.24$$

where θ is the current crank angle, θ_0 the start of combustion, $\Delta\theta$ the total combustion duration in CAD and m_{Wiebe} and a are adjustable parameters. It is worth to indicate that this approximation to the combustion profile is completely unnecessary for the conclusions derived from Equation 3.23 presented in the next paragraph, but it will be a very helpful choice to analyze the effect of the combustion duration on the PC behavior, as will be shown later.

To conclude this theoretical development, Equation 3.23 is quite similar to Equation 3.19, already seen in the previous subsection. The pressure rise is now represented by two terms: a new term related to the heat introduced by the combustion process, and an energy flux associated to the mass transfer (already presented in Equation 3.19). Therefore, to reproduce the jet characteristics after the pre-chamber combustion, it is necessary to preserve both the relation $A_e/(V_{PC}\,N)$ previously discussed, as well as the pre-chamber mass fraction burning rate.

3.2. Validation and discussion

In the current section, the relation between geometrical and operating parameters presented and discussed in the previous section will be validated. The pressure and temperature rise rate, pressure drop and mass flow rate will be evaluated both during the pre-chamber filling and ejection processes.

As depicted in the theoretical development, a similar pressure rise rate in the pre-chambers that comply with the relation $A_e/(V_{PC}\,N)$ and exhibit a similar combustion process is expected to be obtained. Therefore, changes in (a) the pre-chamber volume, (b) the effective flow area and (c) engine speed will be performed to prove this assumption. Moreover, there will be one case that purposely will not comply with the relation $A_e/(V_{PC}\,N)$, highlighting the discrepancy.

As already discussed, the PC combustion process is greatly affected by the local turbulence and residual gas fraction, which in turn are affected by the PC shape and orifice arrangement. However, these phenomena will not be accounted for in this first approach. For this reason, the center of combustion (CA50) is fixed at 10 crank angle degrees (CAD) before top dead center (BTDC) and the combustion duration, defined as the crank angle degrees between 10 and 90% of the PC burned fuel mass (CA10-90), is set to 5 CAD.

A multi-orifice pre-chamber configuration was taken as the baseline case, and it was tested (with the calculation tools presented in Section 2) along with another four single-orifice pre-chambers. Except for pre-chamber PC 2, all geometries comply with the aforementioned relation: $A_e/(V_{PC}\,N)$. Additional pre-chamber specifications are shown in Table 2.

Table 2. Pre-chamber specifications.

	Pre-chamber				
	Baseline	PC 1	PC 2	PC 3	PC 4

Nozzle diameter (mm)	0.70	1.71	0.70	2.10	2.42
Number of nozzles (-)	6	1	1	1	1
V_{PC} (mm^3)	600	600	600	900	600
A_e (mm^2)	2.31	2.31	0.38	3.46	4.62
N (rpm)	2000				4000
$A_e/(V_{PC} * n)$ (m/s)$^{-1}$	0.115	0.115	0.019	0.115	0.115
V_{PC}/V_{MC} (%)	1.84	1.84	1.84	2.76	1.84
Combustion duration (CAD10-90)	5				

The pre-chamber configurations (PC 1 to 4, all of them with single-orifice) were chosen as follows: PC 1 preserve the baseline volume and the effective flow area. PC 2 preserve the nozzle diameter and the baseline volume, evidencing the error when a multi-orifice pre-chamber is tried to be reproduced in this manner. PC 3 increase both volume and flow area. PC 4 preserve the baseline volume and adjust the effective flow area to compensate the engine speed variation.

3.2.1.Pre-chamber filling process

Figure 2 shows the pre-chamber pressure, pressure drop between chambers and the mass flow rate (in kilograms per CAD) divided by the pre-chamber volume during the filling process. The use of kilograms per CAD instead of per second helps not to confuse the interpretation under different engine speed, since the energy flux and the thermodynamic properties are given in terms of CAD. It is clearly seen that PC 2, the only geometry that do not satisfy the aforementioned relation, presents a disparate pressure profile. This occurs due to the lower mass transfer to the pre-chamber than the needed to increase its pressure in the same rate as the baseline. Therefore, the energy associated to the mass flowing into the pre-chamber (here in terms of enthalpy and kinetic energy) needs to be scaled with the pre-chamber volume. In other words, to reproduce with a given pre-chamber the same pressure rise rate than a baseline, the mass flow rate (in kilograms per CAD) to the pre-chamber (which is a function of the flow area and engine speed) must be scaled with its volume and/or engine speed: this is the reason why when the mass flow rate through the PC holes is divided by the PC volume, the same pattern is found for all PC's that satisfy the aforementioned relation (third column of Figure 2).

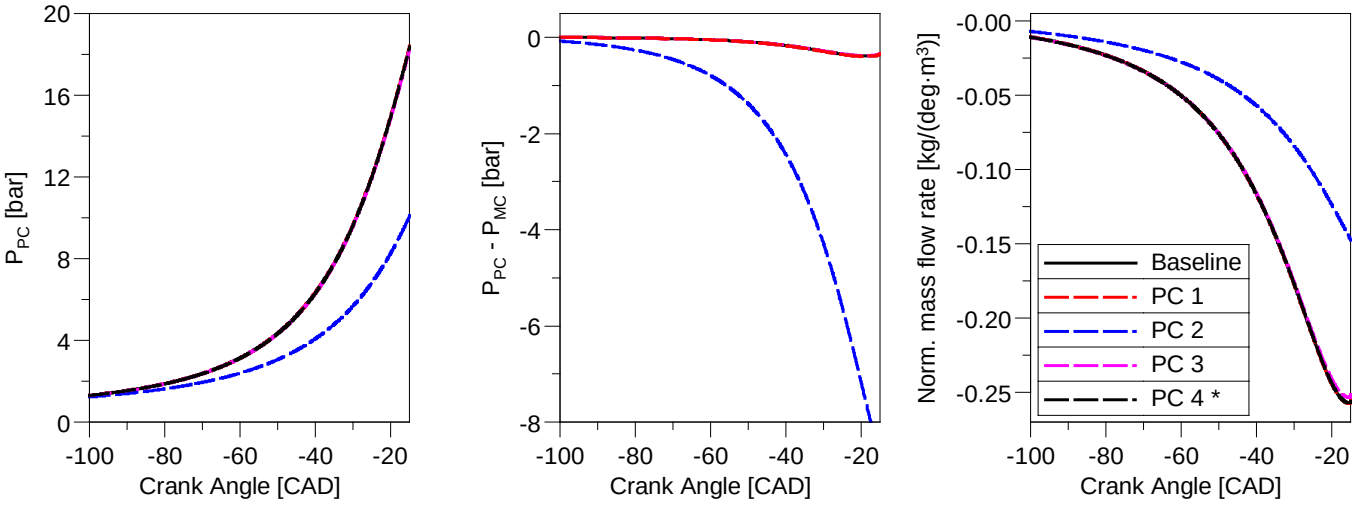

Figure 2 - Pre-chamber pressure, pressure drop and normalized mass flow rate during the pre-chamber filling process. * @4000 rpm.

Since the same initial conditions in the main and pre- chamber are imposed at IVC, and the pressure rise rate is kept the same too, the temperature evolution in the pre-chamber, shown in Figure 3, will naturally be reproduced for the scaled pre-chambers.

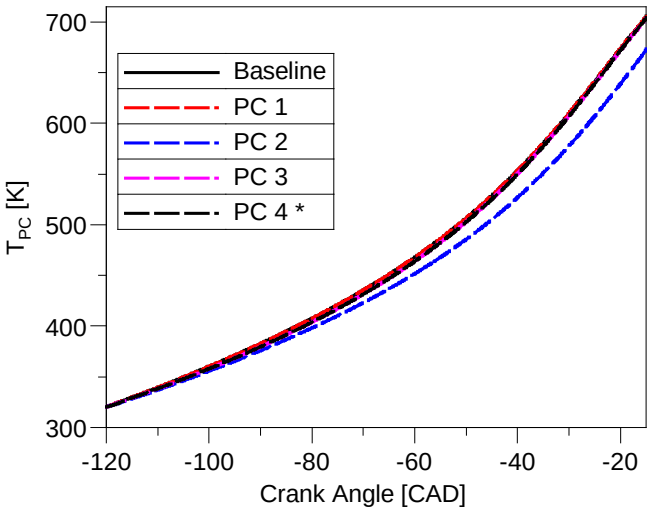

Figure 3 - Pre-chamber temperature during the filling process. * @4000 rpm.

3.2.2.Pre-chamber ejection process

Since the geometrical aspects that govern the mass flow between chambers have just been discussed in the previous subsection, here only the results regarding the pre-chamber combustion and jet ejection will be presented. It is important to note that the burning mass fraction rate ($dx_b/d\theta$ from Equation 3.20) was equally imposed in all pre-chambers, i.e. the center of combustion (CA50) and combustion duration (CA10-90) are equal in all cases.

Figure 4 shows the pre-chamber pressure, the pressure drop from PC to main chamber and the mass flow rate (in kilograms per CAD) divided by the pre-chamber volume during the pre-chamber ejection process. Once again, the pre-chambers that are designed with the same $A_e/(V_{PC}\ N)$ relation present a similar pressure rise rate. As well as in the filling process, the energy exchange between chambers is associated to the mass transfer, which is governed by this geometrical relation previously presented.

Thus, since the rate of burning mass fraction is preserved, the volume necessary to satisfy the relation $A_e/(V_{PC}\ N)$ to a given pre-chamber ensures that the amount of total heat released by the fuel (given by the fuel mass) was the one needed to compensate the energy loss associated to the mass flow rate to the main chamber. This can be seen in Figure 4 to the right, where the mass flow rate divided by the pre-chamber volume (kg/deg·m^3) is preserved in all pre-chambers, except PC 2, evidencing that the heat released by the fuel is counteracted by the mass flow rate, preserving the rate of pressure rise in the pre-chamber during the combustion process.

Although crucial for early flame kernel development and wall induced quenching[33], the PC heat losses represent a small fraction of the total energy available in the pre-chamber. Consequently, small differences in terms of PC geometry that could affect the heat transfer coefficient (surface area to volume ratio, turbulence intensity, and so on) should not influence the pressure rise rate as much as when not satisfying the $A_e/(V_{PC}\ N)$ relation, which is depicted by PC 1 adiabatic in Figure 4.

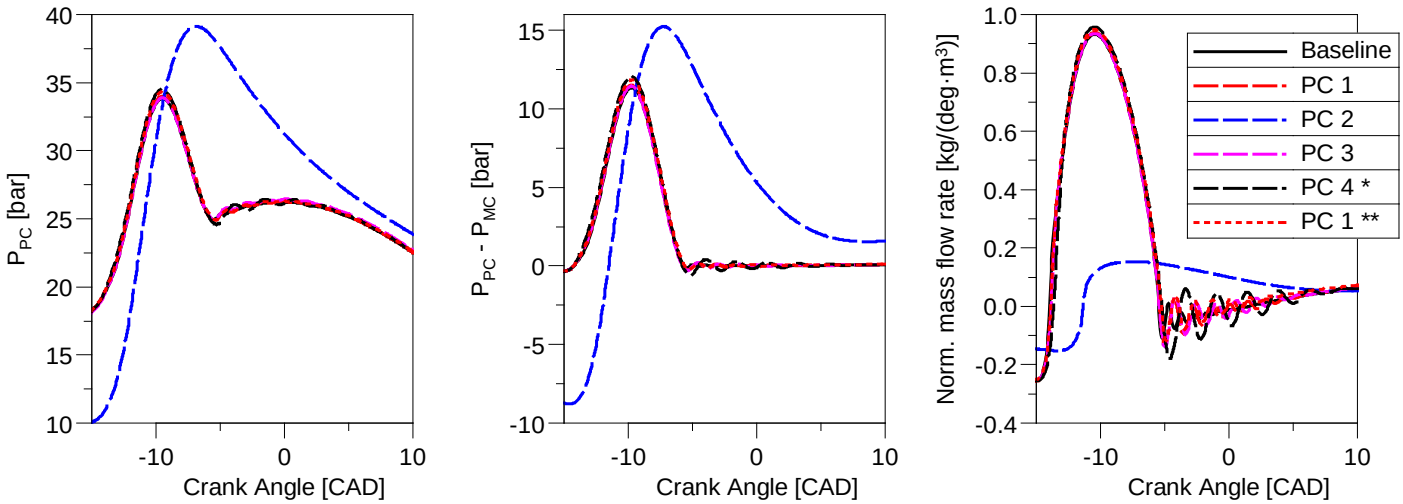

Figure 4 - Pre-chamber pressure, pressure drop and normalized mass flow rate during the pre-chamber combustion process. * @4000 rpm ** Adiabatic.

The disparate PC pressure profile obtained for PC 2 already seen in the previous figure, leads to a dissimilar jet velocity and momentum pattern, as can be seen in Figure 5, where the pre-chambers that satisfy the relation $A_e/(V_{PC}\ N)$ present the same curve shape for these parameters, merely multiplied by a factor that depends on the orifice cross section area in the case of the jet momentum.

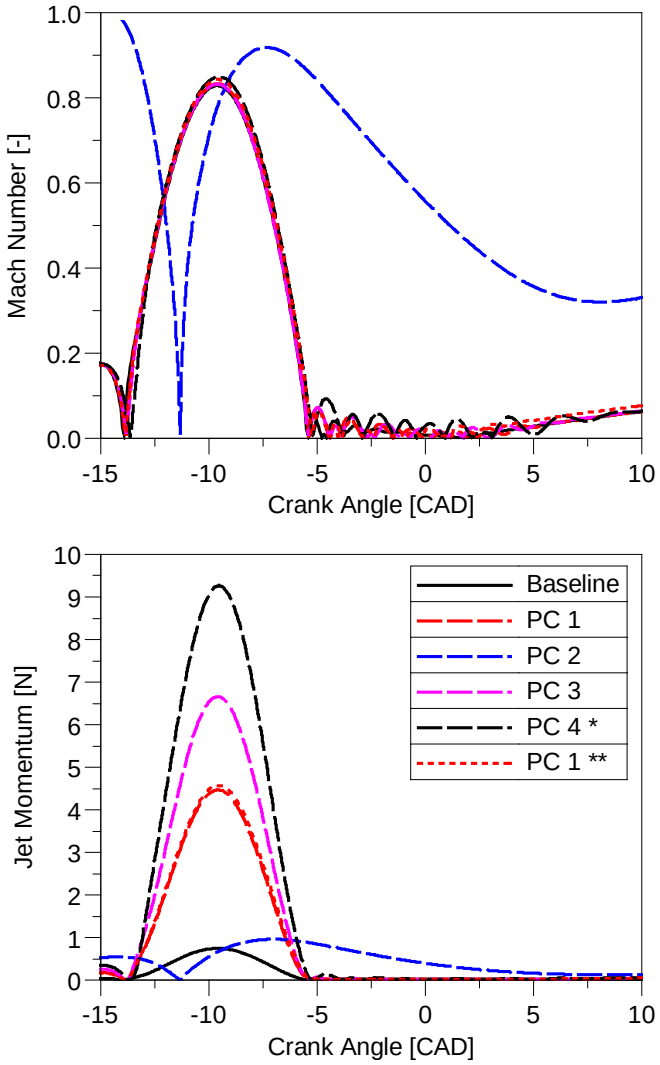

Figure 5 - Mach number and jet momentum. * @4000 rpm ** Adiabatic.

Likewise to the filling process, if the pressure rise rate is kept constant, the temperature evolution in the pre-chamber during the combustion process, shown in Figure 6, will naturally be reproduced for the scaled pre-chambers. Obviously, the adiabatic pre-chamber case presents a higher post-combustion temperature. However, during jet ejection (concomitant with PC combustion), the heat transfer does not seem to have a substantial effect.

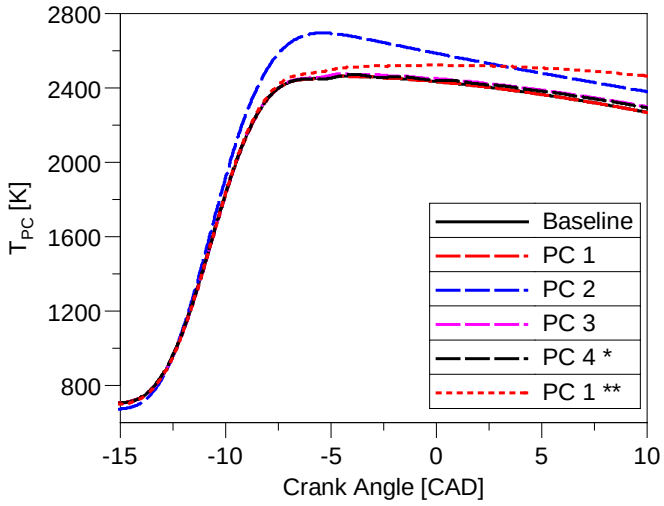

Figure 6 - Pre-chamber temperature during the pre-chamber combustion process. * @4000 rpm ** Adiabatic.

3.2.3.Effect of pre-chamber combustion duration

Here, a brief discussion about the effect of the pre-chamber combustion process is presented. In the previous sub-section, the pre-chamber mass fraction burning rate was assumed to be equal in all cases. However, this might not be the case in some conditions or for some designs, especially when the engine speed of the reference case is quite different to the one of the experimental facility. Thus, to highlight the contribution of the combustion term to the pre-chamber pressure rise rate, as presented in Equation 3.23, a comparison between two combustion durations for the same pre-chamber geometry was done.

Figure 7 presents the pre-chamber pressure, pressure drop and mass flow rate of the two combustion duration cases. The rate of burned mass fraction was changed by means of the combustion duration (the CA50 of this combustion, however, is kept the same), evidencing that a lower rate of burned mass fraction (longer combustion duration) provokes a lower rate of pressure rise in the pre-chamber. Since the total heat released by the fuel is preserved, the energy delivered to the main chamber is preserved too, and only the rate at which this energy is released changes. Thus, different start of jet ejection, ejection velocity and penetration rate are expected.

It can be concluded that the combustion duration must be kept constant when trying to emulate a given reference PC configuration. However, how to ensure this is well beyond the scope of the present research, since this parameter is governed by the local turbulence in the PC, the PC scavenging process, the residual mass fraction, etc., which are not easy to be determined, nor controlled.

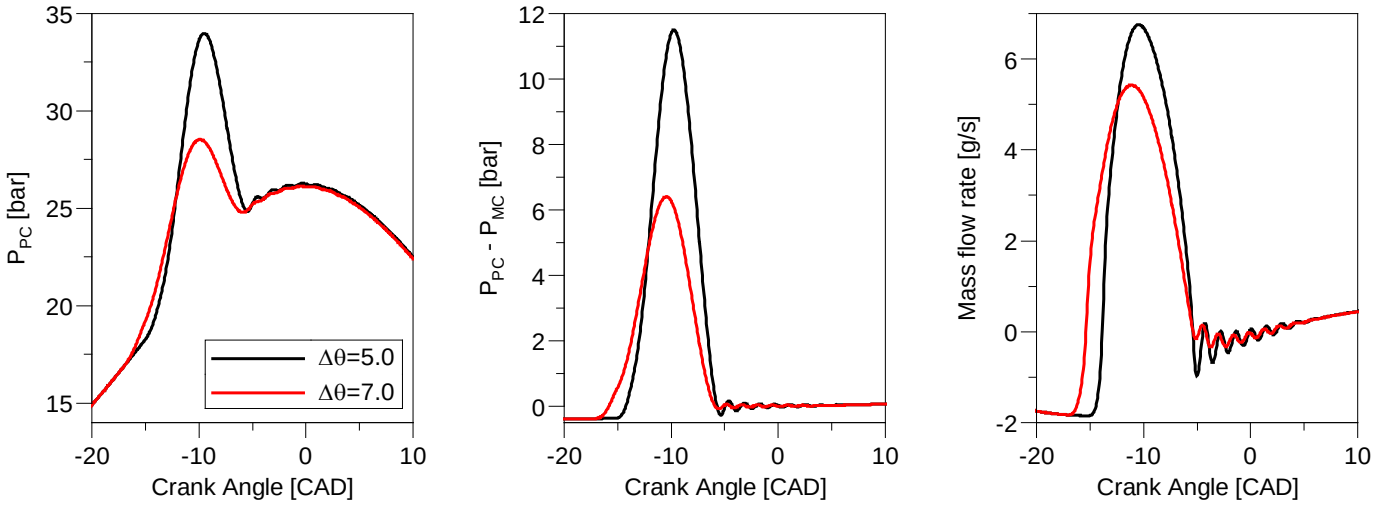

Figure 7 – Pre-chamber pressure, pressure drop and mass flow rate during the pre-chamber combustion process. Effect of combustion duration.

4. Jet penetration

Since how to preserve the pre-chamber thermodynamic conditions was already discussed and validated in previous sections, in this section the jet penetration issue is going to be discussed. Conjointly with the pre-chamber thermodynamic conditions, the jet penetration do play an important role during the main chamber ignition process. Therefore, when a given pre-chamber is emulated under simplified conditions (e.g. single orifice), the relative jet penetration (i.e. normalized by the distance from the orifice to the walls) rate (i.e. penetration per CAD) should be also reproduced.

As proposed by Desantes et al.[34] the jet-tip penetration (s) for a turbulent iso-dense gas jet (i.e. with the same density in both the injected and the ambient gas) can be described as:

$$s = k_p \cdot (d_0 \cdot u_0 \cdot t)^{1/2} \qquad 4.1$$

where k_p, d_0, u_0 and t are a proportionality constant, the orifice diameter, the initial axial velocity at the orifice exit and the time from start of injection, respectively. This equation is valid when the environment is quiescent, the effective Schmidt number is 1, and the jet velocity, the cone angle, the air density, and the jet density are constant during the injection process.

In order to preserve the relative jet penetration rate (per CAD), even under different engine speed, the jet-tip penetration can be normalized by the distance to the walls (L, the distance from the hole exit to the combustion chamber wall along the hole axis), and the time dependency can be transformed into an angular dependency introducing the engine speed (N, in rpm). With these two ideas, Equation 5.1 can be rewritten as:

$$\frac{s}{L} = k_p \cdot \left(\frac{\boldsymbol{d_0} \cdot u_0}{\boldsymbol{L^2}} \cdot \frac{\theta}{\boldsymbol{N} \cdot 6} \right)^{1/2} \qquad 4.2$$

Since the jet velocity (u_0) is preserved when the relation $A_e/(V_{PC}\ N)$ is satisfied, to preserve the relative jet penetration rate (s/L), it is necessary to preserve the relation $d_0/(L^2\ N)$. Thus, even not knowing the exact value of the jet-tip penetration of a baseline PC, it is possible to design a scaled pre-chamber according to the main chamber geometry and engine speed of both configurations: the emulated PC and the PC to be studied in the experimental facility.

As previously discussed in Section 2.2.2, a hypothetical inert jet penetration rate was calculated using a one-dimensional spray model. In this study a constant and equal angle was assumed for all pre-chambers and configurations. Besides, the Schmidt number was assumed as being equal to 1. The jet penetration was estimated for a baseline and two other pre-chambers,

all satisfying the relation $A_e/(V_{PC}\ N)$. PC 1 corresponds to the single orifice configuration with the same volume as the baseline. PC 5 corresponds to the single orifice configuration that reproduces the same relative jet penetration rate as the baseline with twice the engine speed, defined by means of the relation $d_0/(L^2\ N)$. Additional pre-chamber specifications are shown in Table 3.

Table 3 - Pre-chamber specifications. *Suitable chamber length.

	Pre-chamber		
	Baseline	PC 1	PC 5
Nozzle diameter (mm)	0.70	1.71	1.40
Number of nozzles (-)	6	1	1
L	40	62.6*	40*
V_{PC} (mm^3)	600	600	200
A_e (mm^2)	2.31	2.31	1.54
N (rpm)	2000		4000
$A_e/_{(V_{PC}\cdot n)}$ (m/s)$^{-1}$	0.115	0.115	0.115
$d_0/_{(L^2\cdot\ n)}$ (m/s)$^{-1}$	0.0131	0.0131	0.0131
$V_{PC}/_{V_{MC}}$ (%)	1.84	1.84	0.61
Combustion duration (CAD10-90)	5		

Figure 8 shows the jet penetration for the three tested geometries. Comparing the baseline and PC 5, it is noticed that it is feasible to adapt the orifice diameter and the PC volume to achieve the same jet penetration as a reference PC at a different engine speed. The requirements are: (1) to apply the relation $d_0/(L^2\ N)$ to identify the orifice diameter that compensates the engine speed variation and (2) apply the relation $A_e/(V_{PC}\ N)$ to determine the pre-chamber volume. Moreover, if it is necessary to adjust the total penetration according to the size of the combustion chamber, the relation $d_0/(L^2\ N)$ demonstrates that it is proportional to the square root of the increment in orifice diameter, as verified by the case PC 1 ** in Figure 8, which is the penetration of PC 1 divided by the square root of $d_{PC\ 1}/d_{baseline}$.

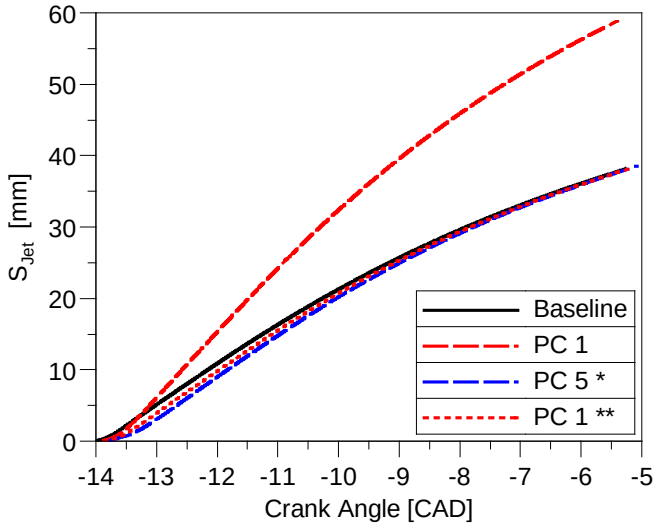

Figure 8 - Jet Penetration. * @4000 rpm. ** Normalized by the distance to the walls (L).

5. Pre-chamber flame quenching

In addition to the physical characteristics, the jet chemical characteristics are crucial for the main chamber ignition process. The question here is whether the flame front can survive or not to the high stretch rate as it passes through the orifice: if the flame can pass through, the jet would be composed by active species that quickly promote the chain-branching in the main chamber; on the contrary, if the flame is quenched, the jet would be composed by unreactive species.

Although the flame quenching is a complex chemical phenomenon and it is extremely challenging to be properly predicted, this section aims to briefly review some criteria used to quantify this phenomenon based on 0D and 1D aspects, and thus incorporate one more important rule to the pre-chamber design process.

The approach traditionally used in SI engines to determine the quenching distance in close to wall regions or in crevices, which is estimated from the balance between the heat released within the flame and the heat loss to the walls [32,35], seems to be not valid to estimate the quenching diameter in pre-chamber applications due to the very large velocity gradients.

Mastorakos et al. [7] observed, by means of experimental and CFD Large Eddy Simulation data, that the flame quenching may be more related to the excessive stretch than to the wall heat transfer in the orifice. In addition, the orifice diameter may lead to exceed the maximum curvature tolerated by the flame front. Although the exact numerical relationship between radius of curvature of the cylindrical flame and flame thickness is not clear at present, the orifice diameter needed to prevent flame extinction is proposed to be at least twice the flame thickness [7].

T. Adams [36] suggested that for a flame to pass through an orifice without being extinguished, the characteristic time of turbulence must be greater than the characteristic time of combustion, leading to a relation between flame thickness (δ), flow velocity at the nozzle (v_0) and flame propagation velocity (v_f), given by:

$$d_0 \geq \frac{\delta v_0}{2 v_f} \qquad 5.1$$

S. Biswas et al. [19] do not correlated the flame quenching at the orifice directly with its diameter. However, they proposed to evaluate the Damköhler number at the orifice exit to characterize the main chamber ignition mechanism. The two mechanisms proposed by the authors are based on the presence or absence of active radicals (e.g. OH) in the jet, which evidence the flame passing or flame quenching at the orifice, respectively. For methane, the authors found that the transition between mechanisms occur at a Damköhler number range between 300 and 350. The use of a

non-dimensional number such as the Damköhler number, allows to transfer this knowledge from test rigs to engine-like conditions.

Therefore, the Damköhler number calculated based on the orifice exit conditions can be used as a flame quenching quantification parameter. For torch ignition systems, where there is no flame quenching at the orifice, the Damköhler number should be at least equal or greater than the reference case, whereas for jet ignition systems, where there is flame quenching at the orifice, the Damköhler number should be at least less or equal than the reference case.

The Damköhler number is the ratio of the characteristic eddy turnover time (τ_T) to the characteristic chemical reaction time (τ_L), as described by:

$$Da = \frac{\tau_T}{\tau_L} = \frac{{l_I}/{u'}}{{\delta_L}/{S_L}} \qquad 5.2$$

where l_I, u', δ_L and S_L are the integral scale (proportional to the orifice diameter), the turbulence intensity (proportional to the jet velocity), the laminar flame thickness and the laminar flame speed (both depend on the composition and thermodynamic conditions), respectively.

When reproducing a multi-orifice reference PC into a single orifice PC using the methodology presented at the previous sections, it is expected that the jet velocity would be preserved and the orifice diameter would be increased. This approach leads to increasing the characteristic turbulent eddy turnover time in comparison to the reference case and, in some cases, could prevent the flame quenching at the orifice when it should occur. Therefore, one of the possibilities to preserve the flame quenching at the orifice is to proportionally increase the characteristic chemical reaction time by adjusting the equivalence ratio. In the previous example, a lower equivalence ratio would provide a thicker and slower laminar flame, increasing the characteristic chemical reaction time and recovering the Damköhler number of the reference case. However, it is worth to mention that modifying the equivalence ratio also has some secondary, but important, effects (i.e. worse conditions to flame propagation at pre- and main chambers) that could affect the PC pressure rise rate.

6. Conclusions

In this work three relations between the geometrical and the engine operating parameters have been identified and presented: $A_e/(V_{PC}\,N)$, $d_0/(L^2\,N)$ and the Damköhler number. The conservation of the first relation between two pre-chambers, assuming a similar pre-chamber combustion process, ensures an identical pre-chamber pressure rise rate in both cases, whereas the conservation of the second relation allows to preserve the relative jet penetration rate even at a different engine speed. This is possible as a result of a scaled mass flowing in and out of the pre-chamber according to its volume, engine speed and distance to the walls, given by the effective flow area determined from those relations. The fulfillment of the third relation, the Damköhler number, guarantees that the flame quenching phenomenon is also reproduced.

Moreover, the following conclusions can be deduced from this study:

- The design criteria presented in this work serves as a guideline to reproduce reference pre-chamber geometries under simplified conditions, keeping as much as possible the flow conditions, the thermodynamic parameters and the jet characteristics.
- For torch ignition systems the Damköhler number calculated based on the orifice exit conditions should be at least equal or greater than the reference case, whereas for jet ignition systems the Damköhler number should be at least less or equal than the reference case.
- The most convenient situation is when a “sector” (i.e. the volume and flow area are divided by the number of orifices) of a multi-orifice PC is reproduced. Only in this way, the Damköhler number and the thermodynamic conditions are preserved simultaneously, maintaining the turbulence intensity and the integral scale, as well as the characteristic chemical time. For any other choice, there will always be a compromise between faithfully reproduce the thermodynamic conditions (preserving

$A_e/(V_{PC}\,N)$) and the relative jet penetration (preserving $d_0/(L^2\,N)$), or the flame quenching phenomenon (preserving the Damköhler number). A possible way to address this problem is to play with the PC parameters so as to correctly reproduce both the thermodynamic conditions and the relative jet penetration, paying also attention to increase the Damköhler number if the reference case works in the flame ignition regime, or to decrease this number if the reference case operates in the jet ignition regime.

- In the case that the sector approach results in a unfeasible (i.e. too small) PC volume, the recommendation is to stablish a minimum volume and then identify the orifice diameter to satisfy the relation $A_e/(V_{PC}\,N)$ to preserve the PC thermodynamic conditions. From this diameter, the Damkohler number needs to be calculated and compared to the reference case, so as to assess if it is necessary any adjustment on the chemical reaction time to maintain the Damköhler number as close as possible to the range representative of its ignition mechanism.
- Although it was not the main objective of this research, the methodology approach presented in this work can be used to transfer information among different engine sizes. For instance, the knowledge of pre-chambers for large bore engines can be transferred to pre-chambers of passenger cars, and vice versa, serving as a design tool to new pre-chamber geometries, regardless of its application.

Acknowledgments

The authors would like to thank different members of the CMT- Motores Térmicos team of the Universitat Politècnica de València for their contribution to this work. This research has been partially funded by FEDER and the Spanish Government through project RTI2018-102025-B-I00.

References

1. Tanoue K, Kimura T, Jimoto T, et al. Study of prechamber combustion characteristics in a rapid compression and expansion machine. *Appl Therm Eng* 2017; 115: 64–71.

2. Attard WP, Blaxill H. A single fuel pre-chamber jet ignition powertrain achieving high load, high efficiency and near zero NOx emissions. *SAE Int J Engines* 2012; 5: 734–746.

3. Bunce M, Blaxill H. Sub-200 g/kWh BSFC on a Light Duty Gasoline Engine. In: *SAE Technical Papers*. Epub ahead of print 5 April 2016. DOI: 10.4271/2016-01-0709.

4. Toulson E, Schock HJ, Attard WP. A Review of Pre-Chamber Initiated Jet Ignition Combustion Systems. *SAE Tech Pap Ser*; 1. Epub ahead of print 2010. DOI: 10.4271/2010-01-2263.

5. Desantes JM, Novella R, De La Morena J, et al. Achieving ultra-lean combustion using a pre-chamber spark ignition system in a rapid compression-expansion machine. In: *SAE Technical Papers*. Epub ahead of print 2 April 2019. DOI: 10.4271/2019-01-0236.

6. Benajes J, Novella R, Gomez-Soriano J, et al. Evaluation of the passive pre-chamber ignition concept for future high compression ratio turbocharged spark-ignition engines. *Appl Energy* 2019; 248: 576–588.

7. Mastorakos E, Allison P, Giusti A, et al. Fundamental Aspects of Jet Ignition for Natural Gas Engines. *SAE Int J Engines* 2017; 10: 2017-24–0097.

8. Tian J, Cui Z, Ren Z, et al. Experimental study on jet ignition and combustion processes of natural gas. *Fuel* 2020; 262: 116467.

9. Li X, Zhang W, Huang Z, et al. Pre-chamber turbulent jet ignition of methane/air mixtures with multiple orifices in a large bore constant volume chamber: effect of air-fuel equivalence ratio and pre-mixed pressure. *Front Energy* 2019; 13: 483–493.

10. Gholamisheeri M, Wichman IS, Toulson E. A study of the turbulent jet flow field in a methane fueled turbulent jet ignition (TJI) system. *Combust Flame* 2017; 183: 194–206.

11. Qing-he L, Bai-gang S, Yong-li G, et al. The effect of equivalence ratio, temperature and pressure on the combustion characteristics of hydrogen-air pre-mixture with turbulent jet induced by pre-chamber sparkplug. *Int J Hydrogen Energy* 2019; 44: 20470–20481.

12. Gentz G, Gholamisheeri M, Toulson E. A study of a turbulent jet ignition system fueled with iso-octane: Pressure trace analysis and combustion visualization. *Appl Energy* 2017; 189: 385–394.

13. Li F, Zhao Z, Wang B, et al. Experimental study of pre-chamber jet ignition in a rapid compression machine and single-cylinder natural gas engine. *Int J Engine Res* 2019; 1–15.

14. Validi A, Schock H, Jaberi F. Turbulent jet ignition assisted combustion in a rapid compression machine. *Combust Flame* 2017; 186: 65–82.

15. Shapiro E, Tiney N, Kyrtatos P, et al. Experimental and numerical analysis of pre-chamber combustion systems for lean burn gas engines. *SAE Tech Pap* 2019; 2019-April: 1–11.

16. Shah A, Tunestal P, Johansson B. Effect of Pre-Chamber Volume and Nozzle Diameter on Pre-Chamber Ignition in Heavy Duty Natural Gas Engines. In: *SAE Technical Papers*. Epub ahead of print 14 April 2015. DOI: 10.4271/2015-01-0867.

17. Shah A, Tunestal P, Johansson B. Scalability Aspects of Pre-Chamber Ignition in Heavy Duty Natural Gas Engines. In: *SAE Technical Papers*. Epub ahead of print 5 April 2016. DOI: 10.4271/2016-01-0796.

18. da Costa RBR, Teixeira AF, Rodrigues Filho FA, et al. Development of a homogeneous charge pre-chamber torch ignition system for an SI engine fuelled with hydrous ethanol. *Appl Therm Eng* 2019; 152: 261–274.

19. Biswas S, Tanvir S, Wang H, et al. On ignition mechanisms of premixed CH4/air and H2/air using a hot turbulent jet generated by pre-chamber combustion. *Appl Therm Eng* 2016; 106: 925–937.

20. Benajes J, Novella R, Gomez-Soriano J, et al. Evaluation of the passive pre-chamber ignition concept for future high compression ratio turbocharged spark-ignition engines. *Appl Energy* 2019; 248: 576–588.

21. Bunce M, Blaxill H, Kulatilaka W, et al. The Effects of Turbulent Jet Characteristics on Engine Performance Using a Pre-Chamber Combustor. *SAE Tech Pap Ser*; 1. Epub ahead of print 2014. DOI: 10.4271/2014-01-1195.

22. Tolou S, Schock H. Experiments and modeling of a dual-mode, turbulent jet ignition engine. *Int J Engine Res*. Epub ahead of print 2019. DOI: 10.1177/1468087419875880.

23. Soltic P, Hilfiker T, Hänggi S. Efficient light-duty engine using turbulent jet ignition of lean methane mixtures. *Int J Engine Res* 2019; 146808741988983.

24. Gentz G, Thelen B, Gholamisheeri M, et al. A study of the influence of orifice diameter on a turbulent jet ignition system through combustion visualization and performance characterization in a rapid compression machine. *Appl Therm Eng* 2015; 81: 399–411.

25. Xu G, Kotzagianni M, Kyrtatos P, et al. Experimental and numerical investigations of the unscavenged prechamber combustion in a rapid compression and expansion machine under engine-like conditions. *Combust Flame* 2019; 204: 68–84.

26. Gholamisheeri M, Givler S, Toulson E. Large eddy simulation of a homogeneously charged turbulent jet ignition system. *Int J Engine Res* 2019; 20: 181–193.

27. Malé Q, Staffelbach G, Vermorel O, et al. Large Eddy Simulation of Pre-Chamber Ignition in an Internal Combustion Engine. *Flow, Turbul Combust* 2019; 465–483.

28. Novella R, Pastor J, Gomez-Soriano J, et al. Experimental and Numerical Analysis of Passive Pre-Chamber Ignition with EGR and Air Dilution for Future Generation Passenger Car Engines. *SAE Tech Pap* 2020; 2020-April: 1–18.

29. Qin F, Shah A, Huang Z wei, et al. Detailed numerical simulation of transient mixing and combustion of premixed methane/air mixtures in a pre-chamber/main-chamber system relevant to internal combustion engines. *Combust Flame* 2018; 188: 357–366.

30. Pastor J V., Javier López J, García JM, et al. A 1D model for the description of mixing-

controlled inert diesel sprays. *Fuel* 2008; 87: 2871–2885.

31. Desantes JM, Pastor J V., García-Oliver JM, et al. A 1D model for the description of mixing-controlled reacting diesel sprays. *Combust Flame* 2009; 156: 234–249.

32. Heywoood JB. *Internal Combustion Engine Fundamentals*. Second. New York, N.Y.: McGraw Hill, 2018.

33. Bardis K, Xu G, Kyrtatos P, et al. A Zero Dimensional Turbulence and Heat Transfer Phenomenological Model for Pre-Chamber Gas Engines. In: *SAE Technical Papers*, pp. 1–28.

34. Desantes JM, Arrègle J, López JJ, et al. Scaling laws for free turbulent gas jets and diesel-like sprays. *At Sprays* 2006; 16: 443–473.

35. Turns SR. *An introduction to combustion: concepts and applications*. 2nd ed. McGraw-Hill, 2000.

36. Adams TG. Theory and Evaluation of Auxiliary Combustion (Torch) Chambers. In: *SAE Prepr*, pp. 2328–2339.

37. Uzun A, Hussaini MY. Investigation of high frequency noise generation in the near-nozzle region of a jet using large eddy simulation. *Theor Comput Fluid Dyn* 2007; 21: 291–321.

Notations

A_e	Effective flow area
A_n	Nozzle flow area
a	Wiebe constant
CA10-90	Crank angle degrees between 10 and 90% of the fuel mass burned
CAD	Crank Angle Degrees
C_D	Discharge coefficient
CV_{MC}	Main chamber control volume
CV_{PC}	Pre-chamber control volume
c_v	Specific heat at constant volume
d_0	Orifice diameter
E_{CV}	Energy of a given control volume
F_R	F/A equivalence ratio
$(F/A)_{stoich}$	Fuel to air ratio (in mass)
h_k	Enthalpy associated to the mass transfer
k_p	Proportionality constant
L	Distance between orifice exit and cylinder walls/piston surface
l_I	Integral length scale
m	Mass transfer between control volumes
m_{Wiebe}	Wiebe constant
N	Engine speed (rpm)
n	Engine speed (rps)
P_{CV}	Pressure
Q_{ch}	Chemical energy released by combustion of the fuel

Q_{CV}	Heat added in a given control volume
R	Gas constant
S_L	Laminar flame speed
t	Time from start of injection
T_{CV}	Temperature in a given control volume
U_{CV}	Internal energy of a given control volume
u_0	Initial axial velocity at orifice exit
u'	Turbulence intensity
V_{CV}	Volume of a given control volume
v	Jet velocity at nozzle exit
v_f	Propagation velocity
v_0	Flow velocity at the nozzle
W_{CV}	Work done by a given control volume
x_b	Fuel mass fraction burned

671 **Greek letters**

γ	Specific heat ratio c_p/c_v
δ	Flame thickness
δ_L	Laminar flame thickness
$\Delta\theta$	Duration of combustion (Wiebe)
θ	Crank angle degree
θ_0	Start of combustion (Wiebe)
ρ	Density
τ_L	Characteristic turbulent eddy turnover time
τ_T	Characteristic chemical reaction time
φ	Flow compressibility function

672